

MICADO: optical configuration, performance and folding

Demetrio Magrin^{*a}, Roberto Ragazzoni^a, David E. Freeman^b, Frank Eisenhauer^c, Niels Tromp^d,
Marco Drost^d, Ramon Navarro^d, Richard Davies^c, Reinhard Genzel^c

^aINAF - Osservatorio Astronomico di Padova, Vicolo dell'Osservatorio 5, 35122 Padova, Italy

^bOptical Design & Engineering Consultant, 12 Sanderstead Hill, S. Croydon CR2 0HA, UK

^cMax-Planck-Institut für extraterrestrische Physik, Postfach 1312, 85741 Garching, Germany

^dNOVA-ASTRON, Oude Hoogeveensedijk 4,7991 PD Dwingeloo, Netherlands

ABSTRACT

MICADO will be the IR imaging camera for the E-ELT. It has been designed to work in conjunction with both SCAO (in the early phase) and LGS-MCAO system MAORY (for which it has been optimized) and delivers diffraction limited quality over about 1 arcmin field of view covering the wavelength range from 0.8 to 2.5 micron. In this paper, we describe the optical configurations and the observing modes, for both the primary and the auxiliary arms, of the current baseline and we show the expected performances and how the optical path can be folded to fit the available limited space in the cryo-chamber.

Keywords: Imaging, Astrometry, Photometry, IR camera, E-ELT, MICADO

1. INTRODUCTION

MICADO is the Multi adaptive optics Imaging CAmera for Deep Observations for the 42m European Extremely Large Telescope (E-ELT) planned to be operational in 2018 at Cerro Armazones (Chile). MICADO will be mounted at Nasmyth focus (F/17.7) of the E-ELT, and is one option for the “first-light” camera. It will take advantage of both single conjugate adaptive optics and multi-conjugate adaptive optics modules to deliver superb imaging at E-ELT diffraction limited quality over a field of view of about one arcmin and covering the spectral range from I to K band. The instrument has been designed to be compact, stable and with gravity invariant rotation allowing high precision astrometry. Moreover, MICADO implements a simple long slit spectroscopic mode at R~3000 designed to have high throughput. A general overview of the instruments can be found in [1]. The camera is split into two arms: the primary arm will provide imaging and, thanks to its stability, superb astrometry over 53 arcsec with a sampling of 3 mas and the auxiliary arm that allows finer sampling at 1.5 mas over 6 arcsec and 12 mas long-slit spectroscopic capability over 17 arcsec. An overview of the MICADO optics is shown in Figure 1.

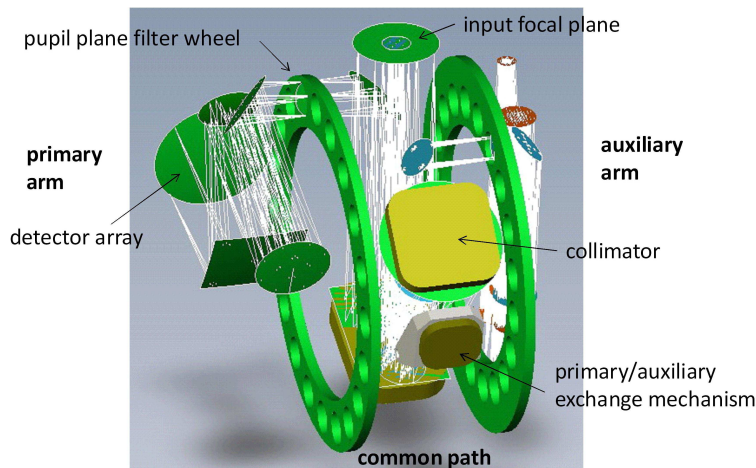


Figure 1. Overview of the MICADO optics.

*demetrio.magrin@oapd.inaf.it; phone +39 049 8293540; fax +39 049 8759840

2. PRIMARY ARM

The primary arm provides imaging and astrometric capability over the spectral bands I-z-Y-J-H-K ($0.78 \mu\text{m} - 2.45 \mu\text{m}$) with diffraction limited quality as delivered by the E-ELT over a field of view of about 53 arcsec. The final PSF quality will be determined by the performances of the two adaptive optics systems: the single conjugate adaptive optics system (SCAO, [2]) based on natural guide stars and multi-conjugate adaptive optics (MCAO) based on laser guide stars (LGS), named MAORY [3, 4]. Only all reflective designs have been considered during the study in order to avoid and minimize color effect, that could invalidate the astrometric measurement precision. On the current design, the only refractive elements are the broad and narrow band filters, the entrance window and the ZnSe/ZnS prisms based atmospheric dispersion corrector (ADC). In this arm, there are no movable mirrors in order to maximize the stability and, therefore the astrometric precision.

2.1 Primary Arm optical design

The primary arm is composed of a single off-axis parabolic mirror, working as collimator and making an image of the pupil where the cold stop is placed, and a camera based on the well-known concept of three mirrors anastigmatic (TMA). The optical layout is shown in Figure 2, where M1 is a parabolic concave mirror, M2 an elliptical concave mirror, M3 a toroidal convex mirror and M4 a spherical concave mirror. In the early phases, when only the SCAO module will be installed, the focal plane array (FPA) is composed by 2×2 detectors (HAWAII-4RG) having a format of 4096 pixels and a gap among them of 5 mm. The pixel size is $15 \mu\text{m}$, giving an FPA size of 127.9 mm. When MAORY will be available, the FPA will be enlarged to 4×4 detectors having the same format, gaps and pixel size, giving a final FPA size of 260.8 mm. The primary arm optical design has been intended to deliver a single plate scale of 3 mas/pixel, i.e. a scale 0.2 arcsec/mm. The correspondent nominal field of views are 25.6 arcsec and 52.2 arcsec for the SCAO module and MAORY respectively. Given the scale of 0.28 arcsec/mm delivered at the E-ELT focal plane, the nominal magnification factor applied by the camera is 1.4. The optical design has been carried out taking into account both the focal plane curvatures delivered by the E-ELT + SCAO system (flat focal plane) and by E-ELT + MAORY system (curved focal plane with curvature radius of 1291.94 mm). In particular, in the last case, the curved focal plane is translated by the camera in another curved focal plane having radius of curvature of 1500 mm. The external detectors of the FPA will mime this shape maximizing the optical quality: the maximum angle of the detector placed at the corner of the FPA have been estimated to be about 5 degrees (the defocus inside each detector is small).

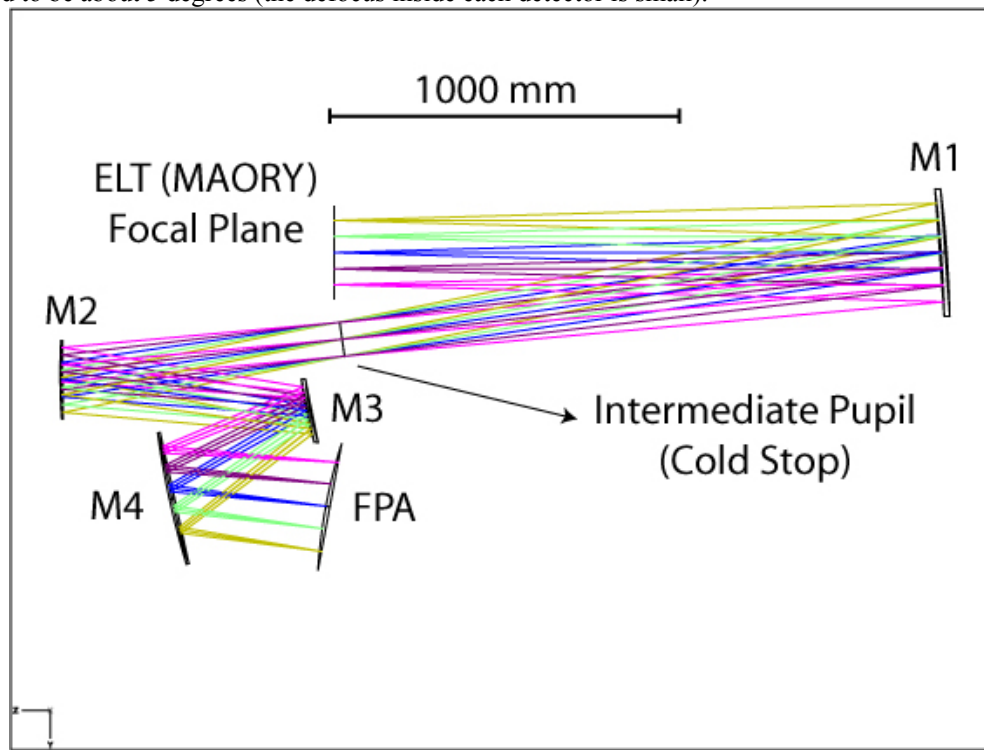


Figure 2. Primary arm optical layout.

In the case of the E-ELT+MAORY, the field distortion over the entire field of view has a maximum value of 1.17%. The effective field of view covered by the FPA can be approximated by an isosceles trapeze having the upper base of 53 arcsec, a lower base of 52 arcsec and a height of 51.4 arcsec.

The nominal optical quality of the primary arm has been estimated for both the AO systems by considering the Strehl ratio maps over the entire field of view at the wavelengths at 0.780, 1.615 and 2.450 μm . The results are shown in Figure 3. During the simulation both the AO systems have been considered to deliver their theoretical PSFs at the camera entrance focal plane. Assuming a perfect correction from AO systems, the worst values of the Strehl ratio are 83.1% and 83.8% at 0.780 μm for the E-ELT+MAORY+Primary Arm and E-ELT+MAORY+SCAO respectively, i.e. the primary arm camera delivers diffraction limited quality over the whole field of view.

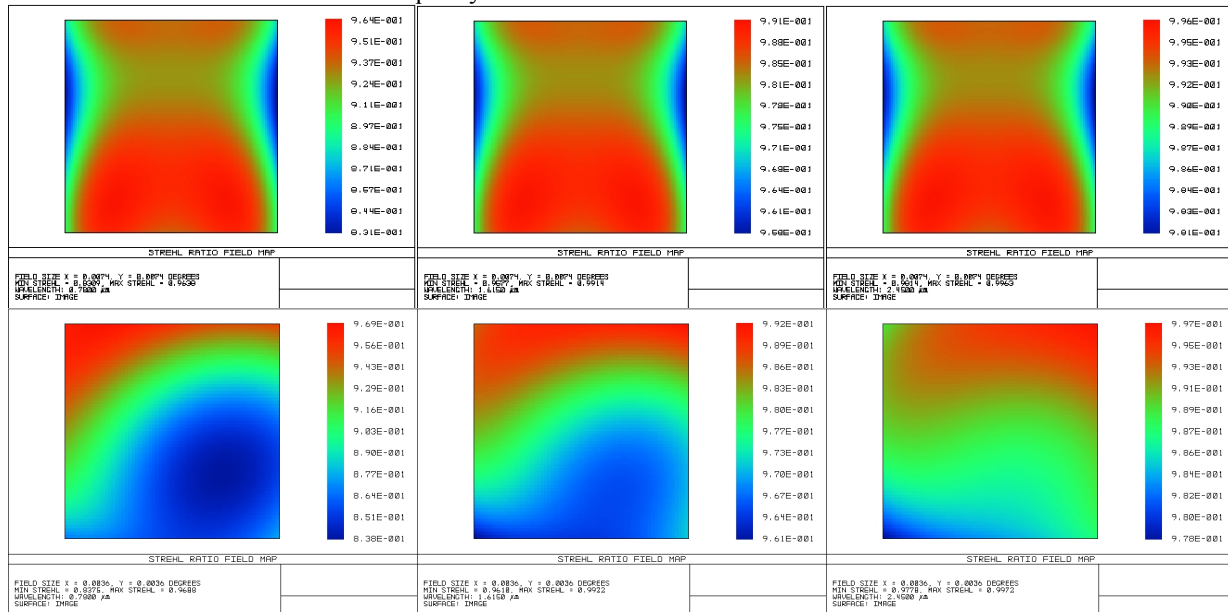


Figure 3. Strehl ratio map over the entire field of view at 0.780, 1.615 and 2.450 μm (columns) for the E-ELT+MAORY+Primary Arm (first row) and E-ELT+SCAO+Primary Arm (second row).

The maximum circle circumscribing the intermediate pupil has a diameter of 100.5 mm. The pupil shape varies with field position. In order to minimize the thermal radiation a circular cold stop must be undersized at 99.1 mm (i.e. all the light for the on-axis field is unvignetted). In the worst case, corresponding to the field at the corner, the maximum fraction of light blocked is 0.96%.

Since all the optical elements are mirrors, they do not produce any ghost on the focal plane (we expect to have diffuse light in case of poor mirror roughness). The refractive elements that could cause problems are the filters, the entrance window and the ADC. The filters are placed after the cold stop. To avoid ghosts, it is necessary to tilt the filters with respect to the collimating beam with an angle of about 9 degrees. The ADC presents itself tilted surfaces and should avoid ghosts: an accurate study will be carried out in the future when the ADC parameters and location will be redefined. Assuming a 5 mm thickness ZnSe entrance window (Infrasil is a valid substitute), the expected ghost will be spread on FPA over into a spot having diameter 372 mas (the airy diameter at 1 μm is 12 mas). The area ratio between the ghost spot and a focalized spot is about 1000 times (for thicker window this effect is amplified). Moreover the intensity of the light producing the ghost has to be multiplied by a factor in between $(0.04)^2$ and $(0.02)^2$ depending on the anti-reflection coating efficiency, i.e. the intensity ratio between a ghost and a focalized spot is about 10^{-6} .

A preliminary tolerance analysis has been carried out using as a merit function the PSF Strehl ratio $> 70\%$ at wavelength 1 μm . A list of parameters have been defined corresponding to the errors in positioning (tilts and decenters) and manufacturing for all the mirrors. All the mirrors are assumed to be independent. The location of the detector has been assumed to be adjustable to the best focus position, allowing one to relax the tolerances. For tilts and decenters, tolerances have been computed with respect to the center of each mirror and not to its vertex. More precisely, the local coordinates system has the origin in the intersection between the chief ray of the central field with the optical surface. The 3σ level worst case has a minimum Strehl ratio of 70.4% with the worst tolerances in the mirror position of the order of 0.05 mm.

2.2 Primary Arm folding and mirrors parameters

For compact design and improved stability, the primary arm has been folded in order to have a common entrance optical bench with the auxiliary arm (collimator), to have a separate optical benches for the camera (TMA) and to allow the accommodation of the filter wheel(s) in between the two optical bench, minimizing the required volume. All the optical elements for this arm (except the filters and the ADC) are static. The layouts of the folded primary arm is shown in Figure 4. The radiation incoming from the entrance focal plane has a first reflection in a double-pass fold mirror MF1, then it is collimated by M1 and reflected back toward MF1 itself and reach the second fold mirror MF2. All these mirrors lay over the same optical bench. The intermediate pupil is formed between the fold mirror MF2 and MF3, and in this position will be allocated the cold stop and the filter wheel. The fold mirror MF3 feeds the TMA and these mirrors lie in a common optical bench.

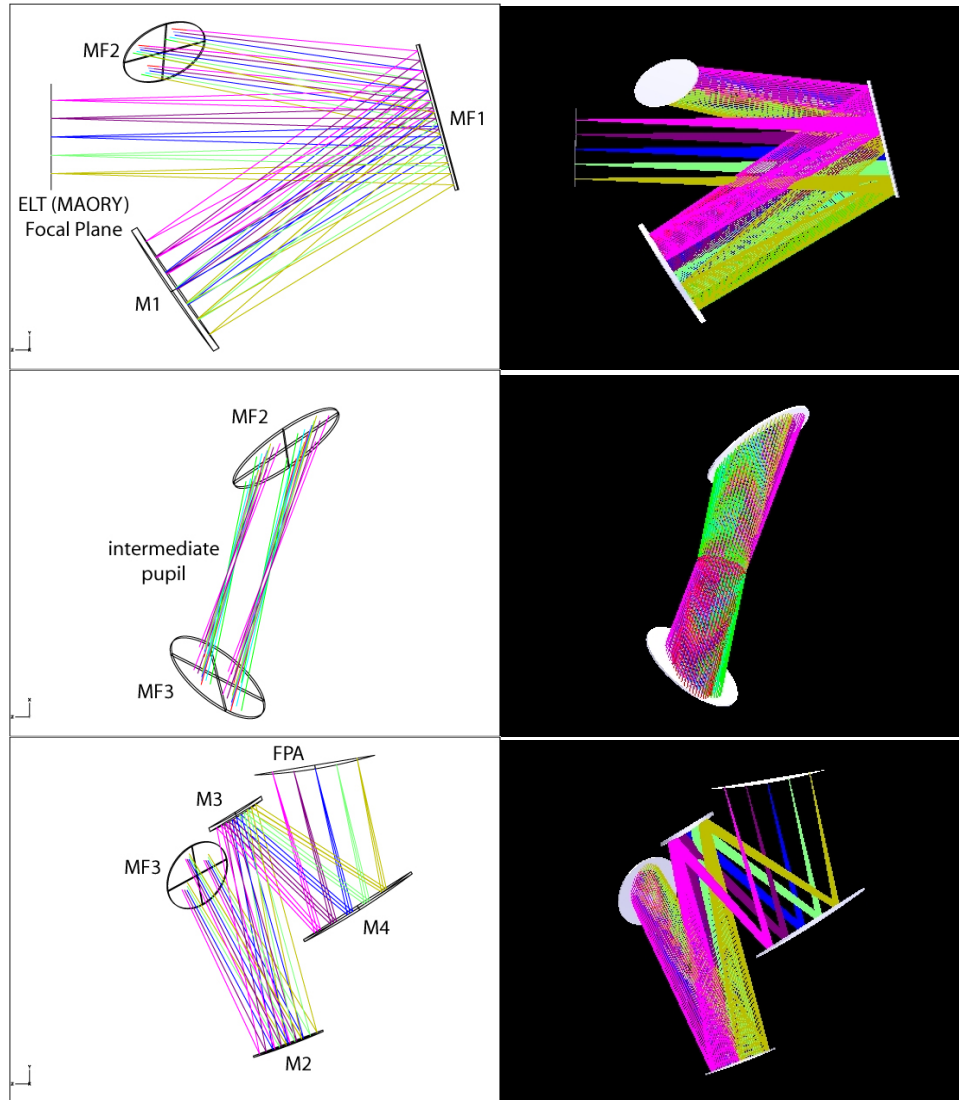


Figure 4. Layout of the folded primary arm. Collimator optical bench (top), cold stop position (middle) and TMA optical bench (bottom). The M_x mirrors are labeled as in Figure 2 while the MF_x mirrors are folding mirrors.

The main parameters for all the primary arm mirrors are given in Table 1. In the Table, the vertex to center distance has been computed assuming as mirror center the intersection between the chief ray of the on-axis field of view and the mirror surface. The positions of the mirrors have been given in global vertex coordinates assuming a coordinate reference linked to the E-ELT + MAORY focal plane.

Table 1. Main parameters (upper) and global vertex coordinates (lower) for the primary arm optical elements.

	R mm	K	Aperture Shape	Clear Aperture mm × mm	Vertex/Center mm
MF1	infinity	-	rectangular	260×380	-
M1	-3474.000	-1	circular	368	-250
MF2	infinity	-	elliptical	230×160	7
MF3	infinity	-	elliptical	160×230	-10
M2	-2043.180	-0.203188	rectangular	196×196	1
M3	-852.566 -843.882	-0.034190 -0.059705	rectangular	144 × 144	210.7
M4	-2449.386	-	rectangular	256 × 276	-12

	Tilt X degree	Tilt Y degree	Tilt Z degree	Decenter X mm	Decenter Y mm	Decenter Z mm
ELT Focal Plane	0	0	0	0	0	0
MF1	15.000	0	0	0	50.000	-980.000
M1	30.000	0	0	0	-171.994	-182.098
MF2	-35.000	45.000	40.000	0	212.390	-280.000
MF3	145.000	45.000	-125.000	-439.341	30.584	-152.887
M2	110.500	0	180.000	-439.341	-483.294	-427.832
M3	107.000	0	180.000	-439.341	121.443	-77.621
M4	122.000	0	180.000	-439.341	-75.849	-629.414

2.3 Atmospheric Dispersion Corrector

Because of the wavelength dependent refractive index of air, the observed altitude of a star varies with wavelength, thus smearing the stars image. This effect can be partially compensated with a so-called atmospheric dispersion corrector made from two pairs of double prisms. We calculated how well this effect can be compensated with a classical ZnSe/ZnSe ADC. The ADC has been design as stand alone, independently by the primary arm; the optical quality of the E-ELT+MAORY+ADC+PRIMARY ARM has been checked *a posteriori*.

The ADC has been assumed to be placed at about 500 mm in front of the delivered focal plane (this is not the ideal location because of the optical elements size, the location will be re-assessed during the preliminary design phase). At this location the diameters of the ADC optical elements result to be about 300mm. The first and the last surfaces of the ADC prisms presents toroidal shapes in order to correct the astigmatism introduced from the rather thick prisms (30 mm) in the convergent beam. The ADC has some residual axial chromatism (focus shift as function of wavelength) but it seems negligible over the single filters pass-bands. The focus shift on the entrance FP introduced by the ADC is expected to be compensated by the AO modules (MAORY/SCAO). The expected dispersion correction performance in the J-band is shown in Figure 5. The correction in H-band and K-band is similar. The optical quality have been checked with the Strehl ratio map over the whole field of view and we obtain a worst case in the H band of 61.5% while it is 77.2% in the K band.

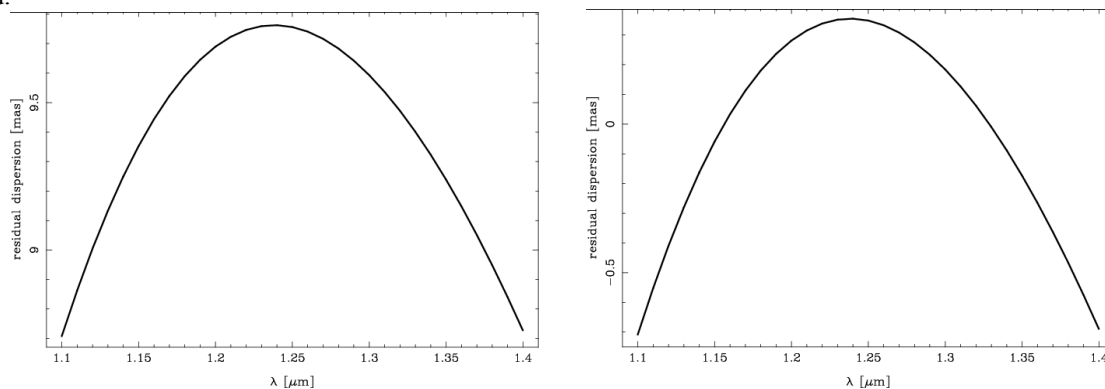


Figure 5. Residual dispersion vs. wavelength assuming a JHK-range ADC tuned to J-band (left) and residual dispersion vs. wavelength assuming an ADC specifically designed for J-band (right).

3. AUXILIARY ARM

The auxiliary arm provides imaging capability with two focal plane samplings (4 mas/pixel and 1.5 mas/pixel) over the same spectral range of the primary arm with diffraction limited quality but in small field of view (16.4 arcsec and 6.1 arcsec). Moreover, it has to provide long slit spectroscopy based on grisms dispersion elements with a resolution of about 3000. As for the primary arm, only all reflective designs have been considered but, in this case, movable mirrors have been inserted on the optical path in order to allow the switch between the two zoom modes.

3.1 Auxiliary Arm optical design

Both the zoom modes take advantage of a common off-axis parabolic mirror working as collimator and pupil re-imager and, as camera, the first mode uses another off-axis parabolic mirror while the second mode uses a direct Ritchey-Chretien mirrors system. The optical layout is shown in Figure 6, where M1 is a parabolic concave mirror, M2(1) a parabolic concave mirror, M2(2) a hyperbolic concave mirror and M3(2) a hyperbolic convex mirror. The FPA is a single detector having format 4096 pixels with pixel size of 15 μm , common to both the zoom modes. The FPA size is then 61.4 mm. Given the scales of 0.27 arcsec/mm for the first zoom mode and 0.1 arcsec/mm for the second zoom mode and by considering 0.28 arcsec/mm delivered at the entrance focal plane, the nominal magnification factor applied by the auxiliary arm is 1.04 and 2.8 respectively. The resulting nominal field of views are 16.4 arcsec for the first zoom mode and 6.1 arcsec for the second zoom mode. For the auxiliary arm, the FPA will not change with the AO module used.

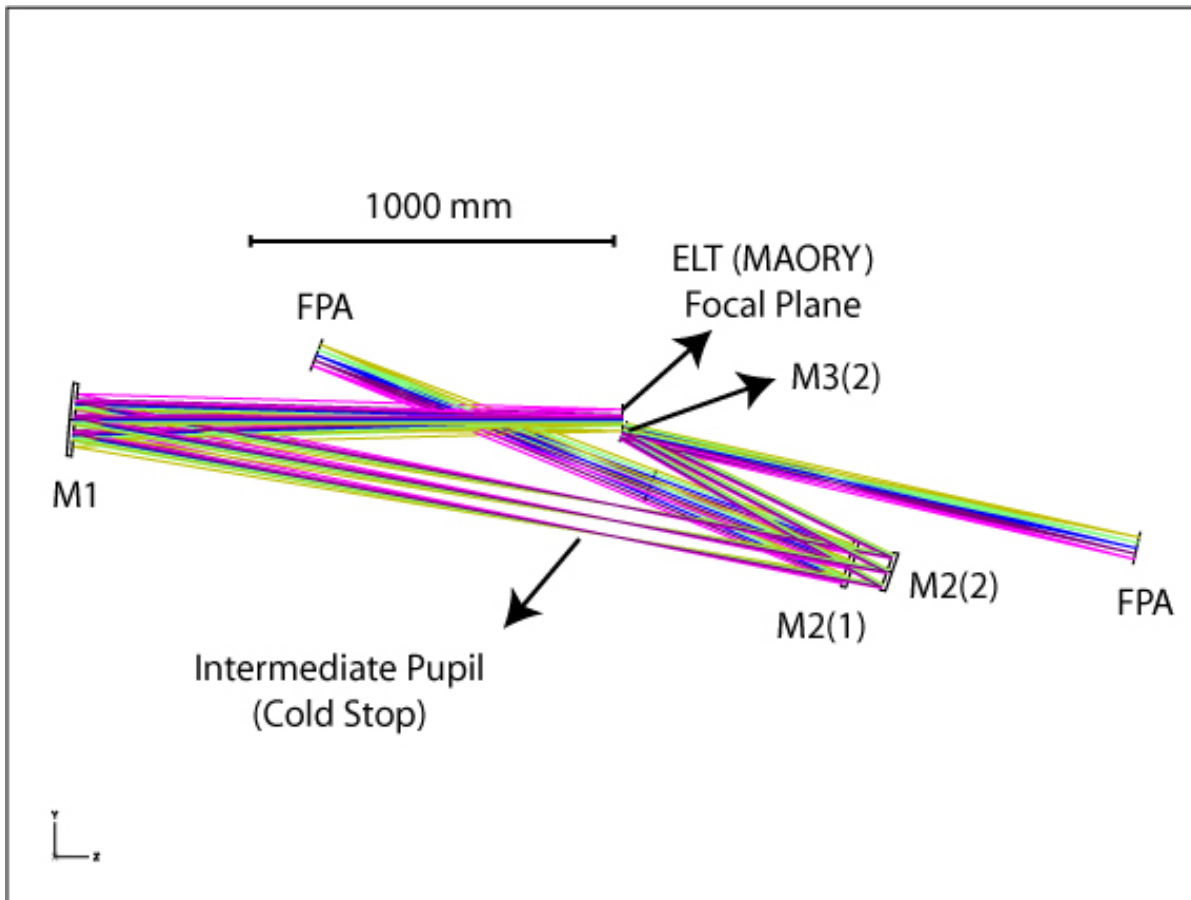


Figure 6. Auxiliary arm optical layout.

In the case of the E-ELT+MAORY, the field distortion over the entire field of view has a maximum value of -0.39% and 0.03% for the first and second zoom mode respectively. The effective field of view covered by the FPA is square with a size of 17.1 arcsec and 6.4 arcsec in the two cases. The nominal optical quality has been estimated for both the AO systems by considering the Strehl ratio maps over the entire field of view at the wavelengths at 0.780, 1.615 and 2.450

μm . In Figure 7 are shown the results for E-ELT+MAORY for both the zoom modes. For the first zoom mode, the worst case is about 61% Strehl ratio at 0.780 μm that is largely better than the expected performance of MAORY at this wavelength. Moreover, the Strehl ratio is higher ($\geq 75\%$) everywhere in the long-slit, for which this mode is mainly intended. The worst case for the second zoom mode at the same wavelength is 89%. In the case of E-ELT+SCAO (not shown in the figure), the worst cases are 77.8% and 81.7% at 0.780 μm for the first and the second zoom modes respectively.

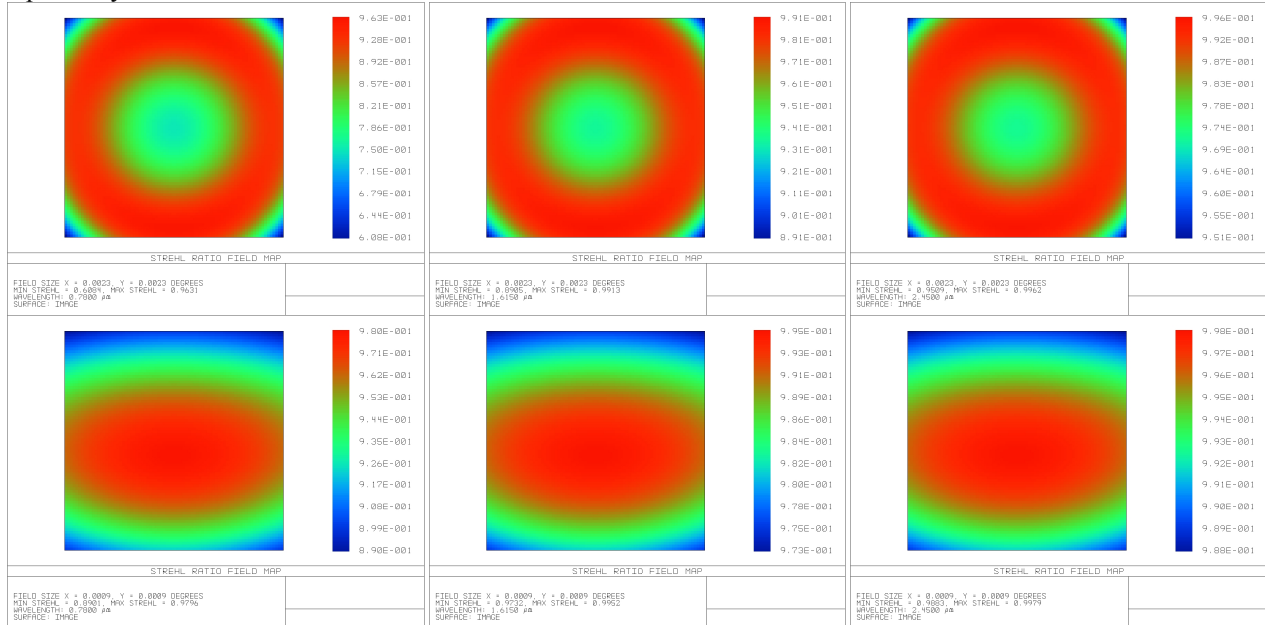


Figure 7. Strehl ratio map in the case of E-ELT+MAORY over the entire field of view at 0.780, 1.615 and 2.450 μm (columns) for the first zoom mode (top) and second zoom mode (bottom).

The maximum circle circumscribing the intermediate pupil has a diameter of 86.3 mm. The cold stop has been undersized to 85.6 mm and, for a field at the corner, the maximum fraction of vignetted light is 0.42%. A preliminary tolerance analysis has done with the same recipe as for the primary arm. The 3σ level worst case has a minimum Strehl ratio of 71.0% and 78.6% for the first and the second zoom modes respectively, with the worst tolerances in the mirror position of the order of 0.05 mm.

3.2 Auxiliary Arm folding and mirrors parameters

The auxiliary arm has been folded in order to have a common entrance optical bench with the primary arm (collimator), to allow the accommodation of a dedicated filter wheel(s) and grisms and to have a separate optical bench for the two cameras with a common detector. The switch between the primary arm and the auxiliary arm is allowed thanks to the insertion of the auxiliary arm collimator (M1) on the common optical path. The layouts of the folded auxiliary arm is shown in Figure 8. The radiation incoming from the entrance focal plane has a first reflection on the double-pass fold mirror MF1, the same used for the primary arm. The auxiliary arm selection is done through the insertion of the collimator M1 that reflects the radiation back toward MF1 till the second fold mirror MF2. All these mirrors lay on the same optical bench (that mounts also the primary arm collimator M1 and fold mirror MF2). The intermediate pupil is formed between the fold mirror MF2 and MF3, and in this position will be allocated the cold stop, the filters and grisms wheel. The fold mirror MF3 feeds the two cameras (zoom modes). The first zoom mode has compound by an off-axis parabolic mirror (M2(1)) and by a fold mirror MF4(1). The second zoom mode has compound by a Ritchey-Chretien mirror system (M2(2) and M3(2)) and by a couple of fold mirrors (M4(2) and M5(2)) that allow the radiation to reach the same detector of the first zoom mode. To switch between the two zoom modes, it is necessary to move out from the beam the parabolic mirror M2(1) and to insert the fold mirror M5(2) and vice versa.

The main parameters for all the mirrors are given in Table 2. In the Table, the vertex to center distance has been computed assuming as mirror center the intersection between the chief ray of the on-axis field of view and the mirror

surface. The positions of the mirrors have been given in global vertex coordinates assuming a coordinate reference linked to the E-ELT + MAORY focal plane.

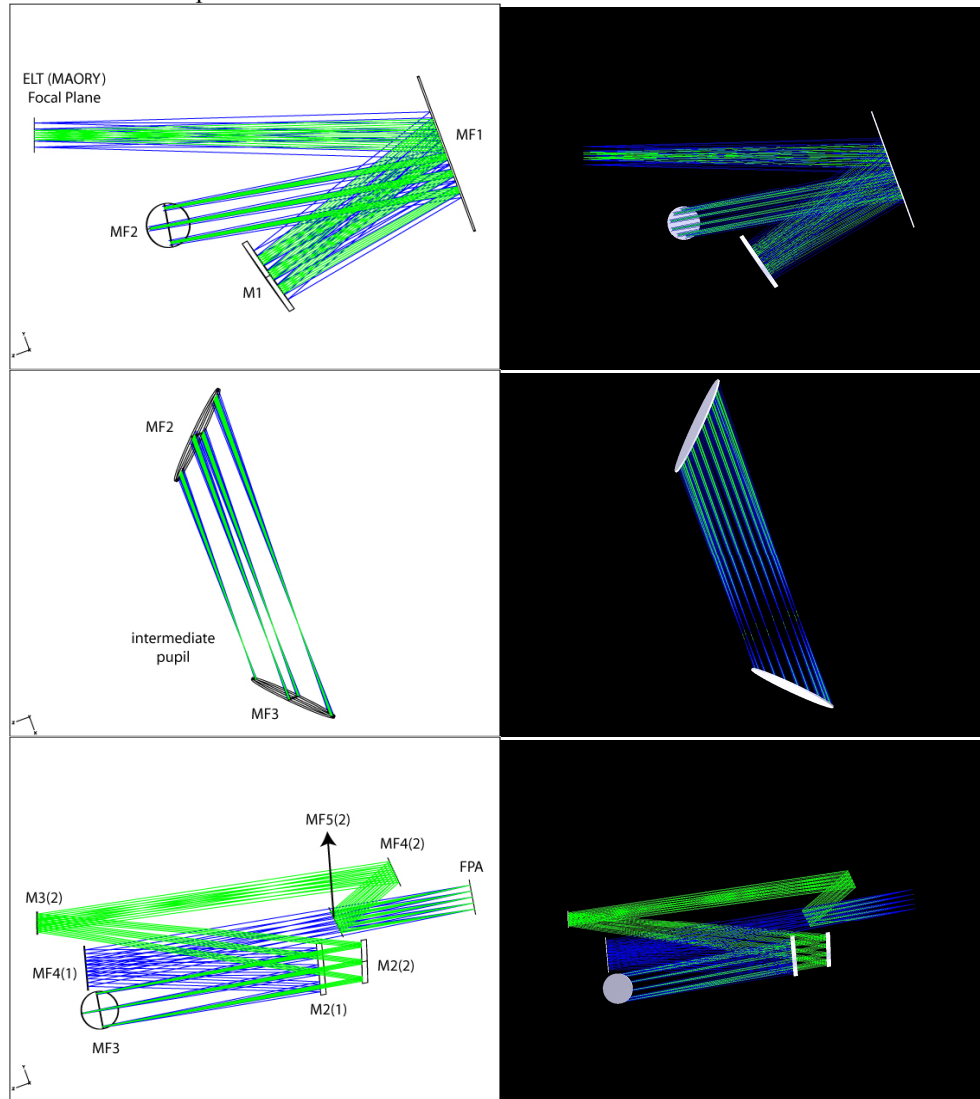


Figure 8. Layout of the folded auxiliary channel. Collimator optical bench (top), cold stop position (middle) and the camera optical bench (bottom). The M_x mirrors are labeled as in Figure 6 while the MF_x mirrors are folding mirrors. The numbers in brackets refer to the zoom mode: (1) for the larger pixel scale, mainly for spectroscopy, and (2) for the finer 0.15 mas scale for oversampling the PSF in extremely crowded fields.

3.3 Auxiliary Arm in spectroscopic mode

The auxiliary arm provides a simple long slit spectroscopic mode. The required resolution is $R=3000$ over the full spectral range with a slit width of 12 mas (i.e. 3 pixels). Preliminary simulations have been carried out based on gratings as dispersion elements. These elements can be located in the filters wheel (near the intermediate pupil) or in a dedicated wheel. The grism material we selected is the ZnSe that guarantee high throughput. The whole spectral range has been divided into 4 sub-spectral bands (I-z, y-J, H, K) covered each one by a dedicated grism. For the first two bands (I-z, y-J) the camera optical quality restrict the resolution between about 1500 to 3000, while for the second two bands (H, K) the resolution can be improved to 2500-4000 with the limitation mainly given by the diffraction size of the PSF. In Figure 9 is shown the simulated resolution for the H band.

Table 2. Main parameters (upper) and global vertex coordinates (lower) for the auxiliary arm optical elements.

	R mm	K	Aperture Shape	Clear Aperture mm × mm	Vertex/Center mm
MF1	infinity	-	rectangular	260×380	-
M1	-3000.000	-1	circular	200	-275
MF2	infinity	-	elliptical	148×108	-
MF3	infinity	-	elliptical	132×96	-
M2(1)	-3119.689	-1	circular	130	-297
MF4(1)	infinity	-	circular	112	-
M2(2)	-2459.474	-1.0168	circular	108	-375.7
M3(2)	-1221.144	-2.1639	circular	56	-115.8
MF4(2)	infinity	-	circular	78	-171.2
MF5(2)	infinity	-	circular	82	-178.4

	Tilt X degree	Tilt Y degree	Tilt Z degree	Decenter X mm	Decenter Y mm	Decenter Z mm
ELT Focal Plane	0	0	0	0	0	0
MF1	15.000	0	0	0	50.000	-980.000
M1	29.500	0	0	0	-108.703	-425.190
MF2	10.500	-45.000	0	0	-220.045	-325.382
MF3	169.500	-45.000	-180.000	401.955	-220.045	-325.382
M2(1)	179.588	0	-180.000	401.955	177.722	-836.453
MF4(1)	-174.956	0	-180.000	401.955	-112.918	-191.271
M2(2)	-169.500	0	-180.000	401.955	258.662	-846.877
M3(2)	-173.934	0	-180.000	401.955	113.041	-63.001
MF4(2)	-155.373	0	-180.000	401.955	267.941	-897.186
MF5(2)	-154.249	0	-180.000	401.955	145.264	-744.351

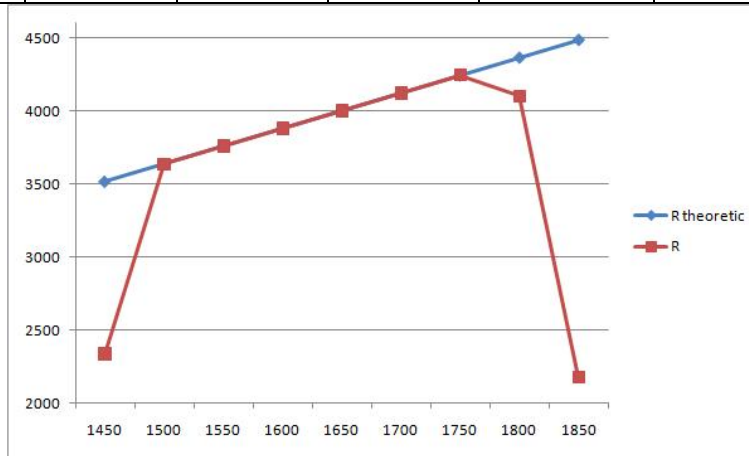


Figure 9. Simulated resolution in the H band.

REFERENCES

- [1] Davies, R. et al., “MICADO: the adaptive optics imaging camera for the E-ELT”, Proc. SPIE, 7735, 80, 2010
- [2] Clenet, Y. et al., “SAMI: the SCAO module for the E-ELT adaptive optics imaging camera MICADO”, Proc. SPIE, 7736, 137, 2010
- [3] Diolaiti, E., et al., in *Adaptive Optics for Extremely Large Telescopes*, eds. Y. Clenet, T. Fusco, G. Rousset, (EDP Sciences) id.02007 (2010)
- [4] Foppiani, I., et al., in *Adaptive Optics for Extremely Large Telescopes*, eds. Y. Clenet, T. Fusco, G. Rousset, (EDP Sciences) id.02013 (2010)